Biomaterials Advances 157 (2024) 213734

Contents lists available at ScienceDirect

Biomaterials Advances

journal homepage: www.journals.elsevier.com/materials-science-and-engineering-c

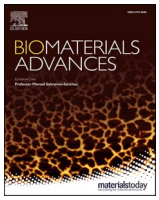

Electrospinning polymersomes into bead-on-string polyethylene oxide fibres for the delivery of biopharmaceuticals to mucosal epithelia

Jake G. Edmans [a,b], Samuel Harrison [b], Paul V. Hatton [a], Craig Murdoch [a,*], Sebastian G. Spain [b], Helen E. Colley [a]

[a] School of Clinical Dentistry, University of Sheffield, 19 Claremont Crescent, Sheffield S10 2TA, United Kingdom
[b] Department of Chemistry, University of Sheffield, Brook Hill, Sheffield S3 7HF, United Kingdom

ARTICLE INFO

Keywords:
Electrospinning
Polymersome
Antibody
Drug delivery
Mucosa

ABSTRACT

Fibrous mucoadhesive polymer membranes prepared using electrospinning demonstrate many advantages for mucosal drug delivery compared to other formulations. Previous electrospun membrane formulations have been developed mainly for the delivery of small molecule drugs. There remains great potential to further develop the technology for the delivery of vesicular vectors that allow administration of advanced therapeutic agents. However, there are no previous reports demonstrating the release of intact drug delivery vesicles from electrospun materials. Here, we describe incorporation and release of protein-loaded polymersomes from polyethylene oxide (PEO)-based electrospun membranes. Polymersomes comprising a copolymer of glycerol monomethacrylate (GMA) and hydroxypropyl methacrylate (HPMA) were prepared using polymerization-induced self-assembly and incorporated within PEO membranes using bead-on-string electrospinning at approximately 40 % w/w by polymer mass. Super-resolution fluorescence imaging showed that the vesicles remained intact and retained their encapsulated protein load within the fibre beads. Transmission electron microscopy and dynamic light scattering demonstrated that polymersomes retained their morphology following release from the polymer fibres. F(ab) antibody fragments were encapsulated within polymersomes and then electrospun into membranes. 78 ± 13 % of the F(ab) remained encapsulated within polymersomes during electrospinning and retained functionality when released from electrospun membranes, demonstrating that the formulation is suitable for the delivery of biologics. Membranes were non-irritant to the oral epithelium and fluorescence microscopy detected accumulation of polymersomes within the epithelia following application. This innovative drug delivery approach represents a novel and potentially highly useful method for the administration of large molecular mass therapeutic molecules to diseased mucosal sites.

1. Introduction

Diseases affecting oral mucosal epithelia are highly prevalent and often debilitating. Autoimmune or dysregulated inflammatory conditions are a cause of chronic painful mucosal ulcers, while oral epithelial malignancies can be life threatening [1–3]. Topical treatment options are restricted by the limited range of therapeutic agents that can be delivered using traditional dosage forms, such as buccal tablets, mouthwashes and ointments, which offer little site-specificity and result in short exposure times and off-target toxicity [4]. Fibrous membrane formulations prepared using electrospinning have recently attracted attention for oromucosal, nasal, vaginal and ocular drug delivery because of their flexibility and high surface area, which allows these membranes to conform to curved and dynamic surfaces [5–7]. Their high surface area facilitates efficient drug release and a large number of mucoadhesive interactions with the tissue, leading to prolonged residence time [5]. These oral membranes and patches are highly acceptable to patients, [8] and have recently been translated for clinical use for the delivery of corticosteroids or tacrolimus [9,10].

Previous research on electrospun mucoadhesive membranes has primarily focussed on enhancing the delivery of small molecule drugs, which diffuse unassisted through the tissue following release. However, more advanced treatment options could be introduced by further developing the technology to release non-viral vesicular delivery vectors. Topical delivery of biologics, including protein and nucleic acid-based therapies, may be greatly improved by encapsulation within

* Corresponding author.
E-mail address: c.murdoch@sheffield.ac.uk (C. Murdoch).

https://doi.org/10.1016/j.bioadv.2023.213734
Received 11 October 2023; Received in revised form 28 November 2023; Accepted 11 December 2023
Available online 12 December 2023

tissue-penetrating vesicles that allow passage across the oral epithelium permeability barrier whilst protecting biologics from denaturation [11]. Additionally, vesicles offer the potential for targeted delivery. For example, selectively targeting malignant cells may enable new chemo-preventative treatments, while the ability to target the cytoplasm could introduce new possibilities for mucosal vaccines or anti-inflammatory therapies [12–14].

Polymersomes (PS) are vesicle drug-delivery vectors formed by the self-assembly of amphiphilic block *co*-polymers [15]. In comparison to liposomes, the membrane thickness and chemistry can be tailored more extensively to influence circulation time and drug-release kinetics [16]. Furthermore, physicochemical properties or specific biological interactions involving the hydrophilic block can be used to influence drug distribution. Stimuli-responsive chemistries to pH, temperature or redox reactions can be used to enable intracellular or tissue-specific release [14,17]. The electrospinning of emulsions and dispersions is challenging due to the tendency for phases to separate in the Taylor cone [18]. Despite this, there have been some successful attempts to encapsulate various types of vesicles using uniaxial or coaxial electrospinning [19]. Alternatively, vesicles can be introduced by coating the fibres after electrospinning [20]. To our knowledge there have been no reports of electrospun materials for the release of intact PS.

Here, we report for the first time the efficient and non-denaturing electrospinning of biologic-loaded PS and their release from electrospun fibres with intact vesicle morphology and biologic functionality. This formulation could form the basis for new therapeutic delivery strategies to treat a variety of topical conditions. This is the first report of bead-on-string electrospinning being used to facilitate encapsulation and provides a major advance for difficult-to-electrospin drug-material combinations.

2. Methods

2.1. Materials

Glycerol monomethacrylate (GMA) was kindly donated by GEO Specialty Chemicals, Hythe, UK. 2-hydroxypropyl methacrylate (HPMA) was purchased from Alfa Aesar, UK. Methacryloxyethyl thiocarbamoyl rhodamine B was purchased from Polysciences, Hirschberg an der Bergstrasse, Germany. 2,2′-Azobis[2-(2-imidazolin-2-yl)propane]dihydrochloride (VA-044) was purchased from Wako Specialty Chemicals, Neuss, Germany. Ethanol, dichloromethane (DCM), and dimethylformamide (DMF) were purchased from ThermoFisher, Loughborough, UK. Poly(ethylene oxide) (PEO), bovine serum albumin (BSA), 4′-Azobis-4- cyanopentanoic acid (ACVA), 2-cyano-2-propyl benzodithioate (CPDB), d-methanol, d-acetone, Sepharose CL-2B, Sephadex G-25, IgG from rabbit serum, 7-hydroxy-4-(trifluoromethyl)coumarin, and all cell culture reagents were purchased from Sigma Aldrich, Gillingham, UK. Mouse IgG and biotinylated goat anti-mouse F(ab) (B-F(ab)) were purchased from Abcam, Cambridge, UK. Other Enzyme-linked immunosorbent assay (ELISA) reagents were purchased from Biotechne, Abingdon, UK.

2.2. ^{1}H Nuclear magnetic resonance spectroscopy

All nuclear magnetic resonance (NMR) spectra were recorded using a 400 MHz Bruker Avance-400 spectrometer and 64 scans were averaged per spectrum.

2.3. Gel permeation chromatography

Analyte samples were prepared at approximately 0.5 % w/w in DMF (HPLC, 0.1 mg/mL LiBr) using 0.1 % v/v toluene as a flow rate marker and filtered through a 0.45 μm polytetrafluoroethylene filter. Analysis was performed using a PL-GPC 50 system fitted with 2 × PLgel Mixed-C 5 μm (300 × 7.5 mm) columns (Agilent, Cheadle, UK). The equipment was calibrated using near-monodisperse poly(methyl methacrylate) standards (5.45×10^2–2.00×10^6 g/mol). Molar mass and dispersity were calculated with Agilent GPC software.

2.4. RAFT synthesis of $PGMA_{45}$ macro-CTA agent in ethanol

Macro-CTA synthesis was performed as previously described [21]. An oven-dried round-bottomed flask was charged with GMA (30.0 g; 187 mmol), CPDB (0.830 g; 3.00 mmol), ACVA (210 mg, 0.196 mmol) and anhydrous ethanol (50 mL), sealed, purged with N_2 for 30 min and placed in a pre-heated oil bath at 70 °C with stirring for 150 min. The reaction was quenched by exposure to air and cooled in an ice bath. The resulting PGMA macro-CTA (GMA conversion = 65 %; M_n = 12,300 g/mol, M_w/M_n = 1.23; Fig. S1, Fig. S2) was purified by precipitation into excess DCM. A mean DP of 45 was calculated using ^{1}H NMR spectroscopy in d-methanol by comparing the integral from 3.4 ppm to 4.3 ppm assigned to the five protons on the PGMA units to that of the aromatic signals at around 7 ppm assigned to the five protons on the RAFT CTA end-group, as previously described [21].

2.5. Preparation of empty $PGMA_{45}PHPMA_{230}$ polymersomes via RAFT aqueous dispersion polymerization for electrospinning optimisation

Polymersomes (PS), were prepared without protein encapsulation using polymerization-induced self-assembly (PISA) based on a previously described method [21]. $PGMA_{45}$ macro-CTA (0.200 g, 26.9 μmol), HPMA (0.954 g, 6.20 mmol) and deionised water (5 mL) were added to a sample vial and purged with N_2 for 20 min. VA-044 (0.32 mL, 5 mg/mL in water, 5.0 μmol, CTA/VA-044 molar ratio = 5.4) was added and the solution purged with N_2 for a further 10 min prior to immersion in an oil bath at 37 °C for 8 h. Finally, the polymerization was quenched by cooling to room temperature with subsequent air exposure and reaction mixtures analysed by ^{1}H NMR spectroscopy in d-acetone as previously described [21]. Negligible methacrylate peaks at 5.6 and 6.8 ppm indicated high monomer conversion (Fig. S3). The product was used without purification and diluted as required in deionised water.

2.6. Electrospinning system and membrane fabrication

Electrospun membranes were fabricated using a system comprising a PHD2000 syringe pump (Harvard Apparatus, Cambridge, UK) and an Alpha IV Brandenburg power source (Brandenburg UK Ltd., Worthing, UK) as previously described [22,23]. Plastic syringes (1 mL volume; Henke Sass Wolf, Tuttlingen, Germany) were used to drive the solutions into a 20-gauge blunt metallic needle (Fisnar Europe, Glasgow, UK). Electrospinning with optimised parameters was performed at room temperature with a potential difference of 19.5 kV, a flow rate of 1.5 mL/h, a volume of 5 mL, and a flight path of 17 cm using a rotating mandrel collector with 20 cm circumference at 100 rpm. Optimised electrospinning solutions were prepared by adding 600 kDa PEO (3 % *w/v*) to deionised water or purified PS solution (within 6 h following purification) and mixing for 18 h.

2.7. Scanning electron microscopy

Electrospun fibres were imaged using a TESCAN Vega3 scanning electron microscope (SEM; Tescan, Cambridge, UK). Samples were sputter coated with gold and imaged using an emission voltage of 5 kV. All images were processed using ImageJ software tools. Fibre and bead diameters were measured by ImageJ using randomly generated co-ordinates and a superimposed grid to randomly select areas to measure [24]. Three independently prepared membranes were analysed for each composition with at least 10 measurements per sample.

2.8. Preparation of Alexa Fluor™ 647-F(ab)

IgG from rabbit serum (8 mg/mL, 0.5 mL) was fragmented into F(ab) (ThermoFisher Scientific, Loughborough, UK) as per the manufacturer's instructions. Low molecular weight impurities were removed using a Vivaspin 30 kDa cut-off centrifugal concentrator (Scientific Laboratory Supplies, West Bridgford, UK). Fragmentation products were analysed without reduction or denaturation by SDS-PAGE using a NuPAGE™ 4–12 % bis-tris gel with MOPS running buffer (ThermoFisher Scientific, Loughborough, UK) and visualised using Expedeon InstantBlue™ stain (Abcam, Cambridge, UK) (Fig. S4). Buffer exchange into 0.1 M pH 8 carbonate-bicarbonate buffer was performed on the F(ab) product using a Zebra™ desalting column (ThermoFisher Scientific, Loughborough, UK) yielding a volume of approximately 0.7 mL. AlexaFluor 647 NHS ester (0.1 mL, 10 mg/mL in DMSO) was added under vigorous stirring and the reaction mixture incubated 1 h in the dark. AlexaFluor 647-F (ab) (647-F(ab)) was purified using size exclusion chromatography (SEC) with Sephadex G-25 and phosphate-buffered saline (PBS). The concentration and degree of labelling (DOL = 3.0) of the resulting F(ab) were estimated from absorbance at 650 nm and 280 nm (assuming a protein molecular weight of 50 kDa and extinction coefficient of 1.4 mL mg^{-1} cm^{-1}).

2.9. Preparation of fluorescent protein-loaded $PGMA_{48}PHPMA_{230}$ polymersomes via RAFT aqueous dispersion polymerization at 20 % w/w solids

Protein-loaded PS were prepared using PISA based on previously described methods [21]. $PGMA_{45}$ macro-CTA (0.100 g, 13.5 μmol), HPMA (0.447 g, 3.10 mmol; Alfa Aesar, UK), BSA (0.133 g), methacryloxyethyl thiocarbamoyl rhodamine B fluorescent monomer (0.25 mg, 375 nmol), aqueous F(ab) solution as required (250 μg biotinylated (B)-F(ab) or 1 mg 647-F(ab)), and deionised water (up to a total aqueous volume of 2.5 mL) were added to a sample vial and purged with N_2 for 20 min. VA-044 (0.16 mL, 5 mg/mL in water, 2.5 μmol, CTA/VA-044 M ratio = 5.4) was added and the solution purged with N_2 for a further 10 min prior to immersion in an oil bath at 37 °C for 8 h. The polymerization was quenched by cooling to room temperature with subsequent air exposure and resulting reaction mixtures analysed by ^{1}H NMR spectroscopy in d-acetone and GPC (Fig. S5, Fig. S6). Negligible methacrylate peaks at 5.6 and 6.8 ppm indicated high monomer conversion (>99 %). Within 24 h following synthesis, undiluted crude PS solution (1 mL) was purified by SEC in deionised water using a Sepharose CL-2B column to collect highly fluorescent fractions (approximately 4 mL). Concentration of the resulting purified PS solution was determined using fluorescence spectroscopy using standard curves with fluorescence measured at 548 excitation and 570 nm emission using a spectrophotometer (Tecan, Männedorf, Switzerland). Purified PS concentrations were interpolated from linear standard curves constructed from crude solutions.

2.10. Fourier transform infrared spectroscopy

Fourier transform infrared (FT-IR) spectra were recorded using a PerkinElmer Paragon 1000 FTIR instrument with ATR accessory (PerkinElmer, Beaconsfield, UK) by performing 16 concurrent scans between 800 and 4000 cm^{-1} with a resolution of 2 cm^{-1}.

2.11. Differential scanning calorimetry

Measurements were performed using a Perkin Elmer Pyris 1 calorimeter (PerkinElmer, Beaconsfield, UK). Samples (5 mg) were sealed in aluminium pans and equilibrated at 0 °C before heating to 150 °C at 10 °C/min.

2.12. Mechanical testing

Membranes were cut into test specimens (7 cm × 1 cm) by scalpel, thickness measured using a digital micrometer (Mitutoyo, Kanagawa, Japan), and fitted within a Lloyd LRX mechanical tester with a 2.5 kN load cell (Lloyd Instruments, Bognor Regis, UK), such that the gauge length was 5 cm. Pull-to-break tests were performed at 10 mm/min. Tests were performed in triplicate using independently prepared membranes.

2.13. Preparation and imaging of fluorescent-labelled membranes

7-hydroxy-4-(trifluoromethyl)coumarin (1 mg/mL) was added as a contrast agent to electrospinning solutions prepared as previously described and mixed until homogenous before electrospinning a small volume onto a static electrically-grounded glass coverslip. Coverslips were affixed to slides without mountant and visualised using a Zeiss LSM880 AiryScan confocal microscope. Images containing multiple fibres were acquired in three-channel mode and AiryScan processing applied in 2D. Higher magnification images of individual beads were acquired using the z-stack function in dual-channel mode to prevent photobleaching and by applying 3D AiryScan processing. All images were further processed using ImageJ software tools.

2.14. Transmission electron microscopy

Solutions of approximately 0.1 % *w*/w PS in deionised water were used for TEM images. Copper/palladium TEM grids (Agar Scientific, Stansted, UK) were surfaced-coated in-house with a film of amorphous carbon and made hydrophilic by plasma glow discharge for 30 s before use. Solution (5 μL) was added to the grid for 60 s after which excess was removed with filter paper. Uranyl formate (0.75 % w/w, 5 μL) was added to the gird for 20 s after which excess stain was removed. Finally, the grid was dried using a vacuum line and stored in the dark until use. TEM images were taken using a FEI Tecnai G2 Spirit TEM instrument (FEI Company, Hillsboro, USA) equipped with a Gatan 1kMS600CW CCD camera at 120 kV.

2.15. Dynamic light scattering

Solutions were prepared at approximately 0.1 % w/w in PBS before measuring hydrodynamic particle diameter with a NanoBrook Omni particle analyser using a 25 mW diode laser with a 640 nm wavelength (Brookhaven Instruments, Hallstahammar, Sweden). Data was obtained at a scattering angle of 173°. Each dynamic light scattering (DLS) measurement consisted of 6 runs of 2 min with count rates between 400 and 600 kcps.

2.16. ELISA for the measurement of biotinylated F(ab) concentration

A biotinylated polyclonal goat anti-mouse F(ab) (B-F(ab)) was used as a model protein to assess the suitability of the PS and fibre formulations for the encapsulation of a biologically active antibody fragment. A direct ELISA protocol was used to quantify the antigen binding activity of biotinylated goat anti-mouse F(ab) as previously described [25]. High-binding 96-well plates were coated with mouse serum IgG (10 μg/mL, 100 μL per well) overnight at room temperature and then blocked with BSA (1 % w/v) overnight at 4 °C. To measure unencapsulated F(ab) concentration, samples were diluted 1:1000 v/v in PBS before ELISA loading. To measure total F(ab) concentration, samples were diluted 1:10 v/v in ethanol and mixed briefly by pipette to release PS contents before immediately diluting 1:100 v/v in PBS and loading. Samples and F(ab) standards were incubated for 2 h at room temperature before aspirating and washing three times (0.05 % *w/v* Tween-20 in PBS). Streptavidin-conjugated horseradish peroxidase (50 μg/mL) was added for 20 min before aspirating and washing. Stabilised 3,3′,5,5′-

tetramethylbenzidine/hydrogen peroxide substrate solution was added and incubated at room temperature followed 20 min later by 50 μL per well 2 M aqueous hydrochloric acid to stop the reaction. Optical density was measured at 450 nm with a correction filter reading of 570 nm using a spectrophotometer (Tecan, Männedorf, Switzerland) and concentrations interpolated from 4-parameter logistic standard curves.

2.17. Encapsulation efficiency calculations

Encapsulated F(ab) concentrations are calculated from ELISA measurements by subtracting unencapsulated F(ab) concentration from the total F(ab) concentration as shown in Eq. (1).

$$[F(ab)]_{encapsulated} = [F(ab)]_{total} - [F(ab)]_{unencapsulated} \quad (1)$$

Percentage encapsulation efficiency (%EE) for PS synthesis was calculated as shown in Eq. (2) by performing ELISA measurement on crude PS solutions (diluted as required) and normalising the ELISA measurement of encapsulated F(ab) concentration against the theoretical maximum concentration based on the amount of F(ab) added to the reaction mixture. Additionally, the percentage loss in antigen-binding activity (%AL) during synthesis was calculated using Eq. (3).

$$\%EE = 100 \times \frac{[F(ab)]_{encapsulated}}{[F(ab)]_{max}} \quad (2)$$

$$\%AL_{synthesis} = 100 \times \left(1 - \frac{[F(ab)]_{total}}{[F(ab)]_{max}}\right) \quad (3)$$

Following SEC purification and electrospinning, fibre samples were fully dissolved in PBS at 10 mg/mL at 37 °C for 30 min with shaking and then analysed by ELISA. The total %EE was calculated for the entire fabrication process using Eq. (2), normalising against the theoretical maximum F(ab) loading by dry mass in the resulting fibres. Additionally, the %EE associated with the electrospinning process was calculated using Eq. (4).

$$\%EE_{electrospinning} = 100 \times \frac{\%EE_{total}}{\%EE_{synthesis}} \quad (4)$$

2.18. Estimation of membrane PS content using ^{1}H NMR spectroscopy

Membrane samples were dissolved in deuterated dimethyl sulfoxide (10 mg/mL) and ^{1}H NMR spectra obtained. The integral associated with PEO backbone protons (3.5 ppm) was compared to the integrals of the methacrylate backbone (1.6–2.1 ppm) and pendent methyl group (0.5–1.0 ppm) protons (Fig. S7). The number of protons per monomer unit and the molecular weight per monomer unit were used to calculate PS content within PEO membranes.

2.19. Cell culture and generation of reconstituted human oral epithelium

FNB6-hTERT immortalized oral keratinocytes (FNB6; Ximbio, London, UK) were cultured in a flavin- and adenine-enriched medium consisting of high glucose Dulbecco's modified Eagle's medium (DMEM) and Ham's F12 medium in a 3:1 *v*/v ratio supplemented with 10 % v/v foetal bovine serum (FBS), epidermal growth factor (10 ng/mL), adenine (0.18 mM), insulin (5 μg/mL), transferrin (5 μg/mL), L-glutamine (2 mM), triiodothyronine (0.2 nM), amphotericin B (0.625 μg/mL), penicillin (100 IU/mL), and streptomycin (100 μg/mL). FNB6 cells (5×10^5 in 0.5 mL) were seeded onto the apical surface of fibronectin-coated (10 μg/mL) 12-well, 0.4 μm pore cell culture inserts (Greiner Bio One Ltd., Stonehouse, UK) and cultured submerged for 3 days, after which the reconstituted human oral epithelium (RHOE) models were raised to an air-liquid-interface and cultured for a further 9 days [26].

2.20. Transepithelial electrical resistance

Before measurement, RHOE models were washed with PBS and placed in a 12-well plate, 0.5 mL PBS was added to basolateral chambers and 0.3 mL to apical chambers. Tissue integrity was assessed by measuring transepithelial electrical resistance (TEER) using an EVOM2 voltmeter (World Precision Instruments, Madison, USA) at three locations per model, and the average of these values calculated. The resistance across RHOE was obtained by subtracting the resistance value derived from a blank cell culture insert. TEER was calculated using eq. 5.

$$TEER(\Omega.cm^2) = Resistance(\Omega) \times Epithelium\ area\ (cm^2) \quad (5)$$

2.21. Cytotoxicity testing in reconstituted human oral epithelium

PS-containing membrane samples (10 mg) or PS in solution (1 % w/v, 0.5 mL in PBS) were applied to the apical surface of RHOE. RHOE were wetted with PBS (0.5 mL) to simulate the moisture in the oral cavity. PBS (0.5 mL) was used as non-cytotoxic control; SDS (1 % w/v, 0.5 mL) as a cytotoxic control. After 24 h, samples were removed and the RHOE washed with PBS and cultured for a further 24 h. Finally, RHOE were washed with PBS before adding 3-(4,5-dimethylthiazol-2-yl)-2,5-diphenyltetrazolium bromide (MTT) in media (0.5 mg/mL, 0.5 mL) to both the apical and basolateral chambers and incubating for 3 h. The solution was removed and 0.1 M HCl in propan-2-ol added (1 mL) to the apical and basolateral chambers of each model, with gentle agitation for 10 min to dissolve the formazan crystals. The solutions from the apical and basolateral chambers were combined and absorbance at 570 nm measured spectrophotometrically (Tecan, Männedorf, Switzerland). Percentage viability was calculated by subtracting the average absorbance of the cytotoxic control and normalising relative to the average value of the vehicle controls. The experiment was performed 3 times using different cell passages and independently prepared samples.

2.22. Polymersome delivery to reconstituted human oral epithelium

RHOE were wetted with 0.5 mL PBS to simulate the moisture in the oral cavity, then PS-encapsulated Alexa Fluor™ 647-F(ab)-containing membrane samples (10 mg) or PS in solution (1 % w/v, 0.5 mL in PBS), were applied to the apical surface. After 6 h, samples were removed and the RHOE washed 3 times with PBS before fixing in neutral buffered formalin (10 % w/v) for 24 h. Samples were perfused with 30 % w/v sucrose for a further 24 h before embedding in optimum cutting temperature (OCT) compound (CellPath, Newtown, UK). Frozen sections (20 μm) were collected at −14 °C using a Cryostar NX50 cryostat (ThermoFisher, Loughborough, UK) and mounted in antifade mounting medium with 4′,6-diamidino-2-phenylindole (DAPI; Vector Laboratories, Upper Heyford, UK). Slides were visualised using a Zeiss LSM880 AiryScan confocal microscope followed by processing using ImageJ software tools.

2.23. Data analysis

All statistical analyses and standard curve interpolations were performed using GraphPad Prism 9.3 software (GraphPad Software, La Jolla, USA). Unless stated data are presented as mean ± standard deviation of at least three independent experiments. Unpaired *t*-test or one-way ANOVA with Tukey's post-hoc test was used for pairwise or groupwise comparisons, respectively and results considered statistically significant if $p < 0.05$.

3. Results

3.1. Electrospinning parameters for the encapsulation of polymersomes

To identify suitable electrospinning parameters for PS encapsulation,

empty PS (empty-PS) were synthesized in the absence of protein cargo and used without purification. Electrospinning was attempted at varying voltages with different concentrations of 600 kDa PEO. Electrohydrodynamic processing could not be achieved using 2 % w/v empty-PS solution without PEO for voltages of 15–25 kV (Table 1). Solutions containing 2 % w/v PS with 5 % w/v or 10 % w/v PEO formed a Taylor cone in the presence of an electric field. However, there was excessive accumulation of solution and dripping at the spinneret tip that prevented collection of defect-free material. In contrast, 2 % *w/v* empty-PS with 3 % w/v PEO produced a stable electrospinning jet at 19.5 kV without dripping and a material was collected without visible defects (Fig. S7). For comparison, electrospinning was also performed using PEO solutions in the absence of empty-PS. Electrospinning was achieved for 3, 5, and 10 % w/v PEO. SEM analysis showed that 5 % w/v and 10 % w/v PEO produced smooth monolithic fibres, whereas 3 % w/v resulted in fibres with a high incidence of spindle-shaped beads (Fig. 1).

3.2. Fabrication and physical characterisation of bead-on-string membranes for the encapsulation of protein-loaded polymersomes

BSA was encapsulated by PISA and the resulting fluorescent-labelled BSA-loaded PS (BSA-PS) purified by SEC, yielding dispersions with 2.54 ± 0.33 % w/v BSA-PS. 3 % w/v PEO was added and dissolved to act as a fibre-forming excipient before electrospinning. Based on the dry mass concentrations, the resulting membranes theoretically contained a PS content of 45.8 ± 3.4 % w/w by polymer mass. NMR analysis of membranes dissolved in deuterated DMSO confirmed successful incorporation of PS and showed the membranes contained at least 33 % w/w PS, although this is likely an underestimation due to overlapping signals at 3.5 ppm (Fig. S8). SEM imaging showed that PEO-only membranes comprised bead-on-string fibres with smooth spindle-like beads (Fig. 2Ai). BSA-PS membranes had a similar bead-on-string morphology, except the beads had a bumpy surface (Fig. 2Aii). BSA-PS membranes had a wider fibre diameter of 0.26 ± 0.07 μm diameter in comparison to 0.22 ± 0.05 μm for PEO-only membranes (Fig. 2Bi, $p < 0.05$), although BSA-PS and PEO-only membranes had similar bead diameters of 0.80 ± 0.18 μm and 0.70 ± 0.21 μm, respectively (Fig. 2Bii, $p = 0.06$).

FTIR spectra of both PEO-only and BSA-PEO membranes contained distinctive absorbances associated with the PEO polymer, most prominently C—H stretching at 2890 cm^{-1} and C-O-C stretching at approximately 1100 cm^{-1} (Fig. 2C) [27]. BSA-PEO membranes additionally displayed a broad absorbance at approximately 3400 cm^{-1} associated with O—H stretching and a double peak at 1640 cm^{-1} and 1720 cm^{-1} associated with amide (BSA) and ester (PS) C═O stretching. These indicate successful incorporation of both the BSA-PS polymer and protein.

DSC thermal analysis showed that PEO-only membranes melted at 69 °C (Fig. 2D). BSA-PS membranes had a broader melting peak at 63–66 °C, followed by a decrease in baseline heat-flow, suggesting a depressed PEO melting point, possibly overlapping with a glass transition associated with the PHPMA blocks of PS.

Pull-to-break tensile testing on membrane strips showed that both PEO-only and BSA-PS membranes were highly ductile, with strains at break of 124 ± 41 % and 75 ± 41 %, respectively (Fig. 2Ei). BSA-PS membranes had a significantly lower ultimate tensile strength of 2.64 ± 0.42 MPa compared to 4.15 ± 0.33 MPa for PEO-only membranes (Fig. 2Eii, $p < 0.01$). All membranes were sufficiently strong enough to allow easy handling with forceps (Fig. S7).

Table 1
Electrospinning process development for the incorporation of empty-PS. Electrohydrodynamic processing of a 2 % w/v aqueous PS solution was attempted using varying voltages and concentrations of 600 kDa PEO at a flow rate of 1.5 mL/h and a flight path of 17 cm. For comparison electrospinning of PEO was also performed in the absence of PS.

	0 % PEO	3 % w/v PEO	5 % w/v PEO	10 % w/v PEO
2 % w/v PS	No Taylor cone, 15–25 kV	Stable, 19.5 kV	Excessive dripping, 15–25 kV	Excessive dripping, 15–25 kV
0 % PS	–	Stable, 19.5 kV	Stable, 19.5 kV	Some dripping, 19.5 kV

3.3. Fluorescent imaging of internal fibre structure

To investigate the internal structure of the electrospun fibre formulation. A fluorescent labelled F(ab) (647-F(ab)) was prepared and incorporated into PS (647-F(ab)-PS), which also contained fluorescent-labelled polymer within the hydrophobic interior block. Electrospinning solutions were prepared that contained 7-hydroxy-4-(trifluoromethyl)coumarin as a fluorescent contrast agent to allow imaging of the overall fibre structure.

The fluorescence of the contrast agent revealed the same bead-on-string fibre morphology that was observed by SEM (Fig. 3A). The fluorescence associated with the PS (Fig. 3B) and that of the 647-F(ab) (Fig. 3C) appeared as distinct clusters along the electrospun fibre. Moreover, a compositive image showed that these molecules were co-localised within ovoid beads, showing that the F(ab) remained encapsulated during electrospinning (Fig. 3D) and that the 647-F(ab)-PS accumulate within the fibre bead structures (Fig. 3D). PEO-only and BSA-PS membranes with contrast agent were prepared and imaged identically as controls, showing that there was no spectral overlap between channels (Fig. S9). Optical sections were captured at high magnification showing the internal structure of individual beads (Fig. 3E). On a sub-micron scale the signals associated with the PS hydrophobic blocks and the 647-F(ab) do not overlap. The PS hydrophobic blocks appear as ring-shaped structures approximately 400–700 nm in diameter. The 647-F(ab) appears as spheres approximately 100–300 nm in diameter. Features may appear larger by optical microscopy than by SEM or DLS due to the beads flattening against the surface of the coverslip.

3.4. Morphology of membrane-released polymersomes

Encapsulated BSA-PS were released from the membranes by dissolving in deionised water. A distinctive vesicular morphology, observed by TEM analysis, was preserved following synthesis, SEC purification and release from the electrospun material (Fig. 4A-C). Control, PEO-only membranes displayed no vesicular structures (Fig. 4D).

TEM imaging is somewhat inaccurate for measuring vesicle diameter because of the tendency for soft vesicles to flatten and appear wider when adsorbed to a surface. Therefore, DLS measurements were performed on BSA-PS dispersions in PBS to compare hydrodynamic diameters (Table 2). There was negligible change in diameter following SEC purification and the measurements were in the expected range based on previous findings [21]. Following release from the electrospun membrane, there was no significant change in diameter, however, the standard deviation was increased, likely due to the presence of small PEO macromolecules. Indeed, PEO-only membranes were dissolved and measured as a control, showing a smaller hydrodynamic diameter of approximately 40 nm.

3.5. Encapsulation efficiency using biotinylated F(ab) as a model biopharmaceutical

To act as a model biopharmaceutical, biotinylated polyclonal goat anti-mouse F(ab) antibody fragments (B-F(ab)) were encapsulated within PS (B-F(ab)-PS). During polymerization, radical species can theoretically react with protein thiol groups via the thiol-ene reaction. Therefore, BSA was included as a blocking agent and sacrificial protein to minimise radical-induced denaturation of B-F(ab). The antigen-binding functionality of B-F(ab) to mouse IgG was measured by ELISA.

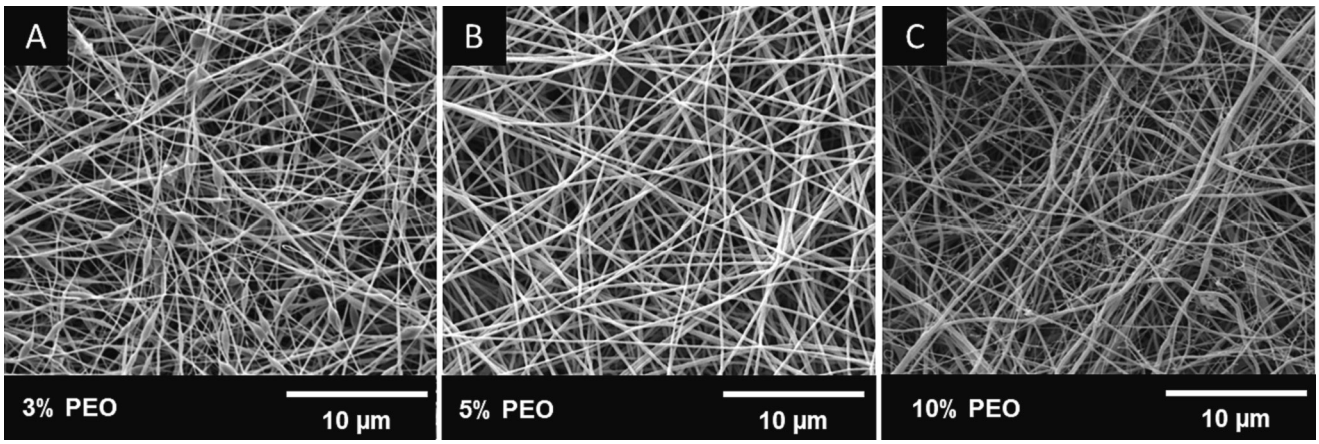

Fig. 1. Scanning electron micrographs of electrospun 600 kDa PEO membranes produced using aqueous solutions at concentrations of (A) 3 % w/v, (B) 5 % w/v, and (C) 10 % w/v. Scale bar = 10 μm.

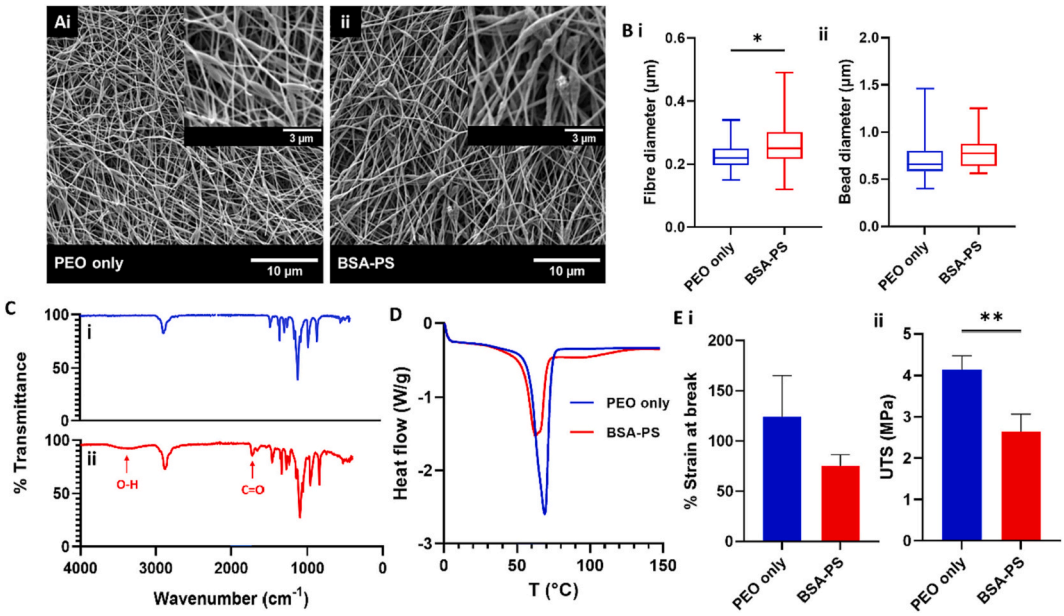

Fig. 2. Morphological and physical characterisation comparing PEO-only and BSA-PS membranes. (A) Representative scanning electron micrographs (SEM) of (i) PEO-only membranes and (ii) BSA-PS membranes (Scale bar = 10 μm) with expansions (Scale bar = 3 μm). (Bi) Fibre diameter and (Bii) bead diameter distributions measured from SEM images, with 10 diameter measurements each for 3 independently prepared membrane samples. Data are presented as median, interquartile range, and range. Pairwise comparisons were made using unpaired *t*-test ($n = 30$). *$p < 0.05$. (C) Infra-red spectra of (i) PEO-only membranes and (ii) BSA-PS membranes. (D) Compared endothermic differential scanning calorimetry traces. (Ei) Strain at break and (Eii) ultimate tensile strength (UTS), obtained by performing pull-to-break tensile testing on 7 cm × 1 cm membranes strips. Pairwise comparisons were made using unpaired t-test ($N = 3$). **$p < 0.01$. (For interpretation of the references to colour in this figure legend, the reader is referred to the web version of this article.)

The total B-F(ab) concentration (including both B-F(ab) contained within B-F(ab)-PS and unencapsulated B-F(ab) in the bulk solution) was detected by lysing B-F(ab)-PS with ethanol before ELISA analysis; unencapsulated B-F(ab) was detected by performing ELISA without lysis.

Analysis of the crude reaction product revealed that 23 ± 10 % of the F(ab) antigen-binding activity was lost during PISA and 36.5 ± 3.1 % of the F(ab) was encapsulated within PS (Table 3). SEC fraction analysis following purification showed that encapsulated B-F(ab) *co*-eluted with the polymer, indicating successful encapsulation within B-F(ab)-PS (Fig. S10). Unencapsulated F(ab) eluted in later fractions, indicating good separation of the unencapsulated B-F(ab). SEC purification yielded polymer concentrations of 2.61 ± 0.53 % w/v that were subsequently electrospun in the presence of 3 % w/v PEO. Based on the dry mass concentrations, the resulting membranes contained 46.5 ± 5.6 % w/w PS by polymer mass and had a theoretical maximum F(ab) loading of 220 ± 21 ng/mg. NMR measurements confirmed that the membranes contained at least 38 % w/w PS. Electrospun membrane samples were dissolved in PBS before performing ELISA analysis, which indicated an EE of 28.5 ± 5.1 % for the entire fabrication process. Therefore, the EE associated with the electrospinning step was calculated at 78 ± 13 %.

3.6. Toxicity testing in reconstituted human oral epithelium

RHOE were used to test the cytotoxicity based on Organisation for Economic Co-operation and Development guidelines for assessing skin irritancy (OECD 439). BSA-PS was applied as a solution (0.5 mL, 1 % w/v) or electrospun membrane (10 mg, with 0.5 mL PBS). Neither the BSA-PS applied as solution nor as a membrane reduced cell viability (Fig. 5).

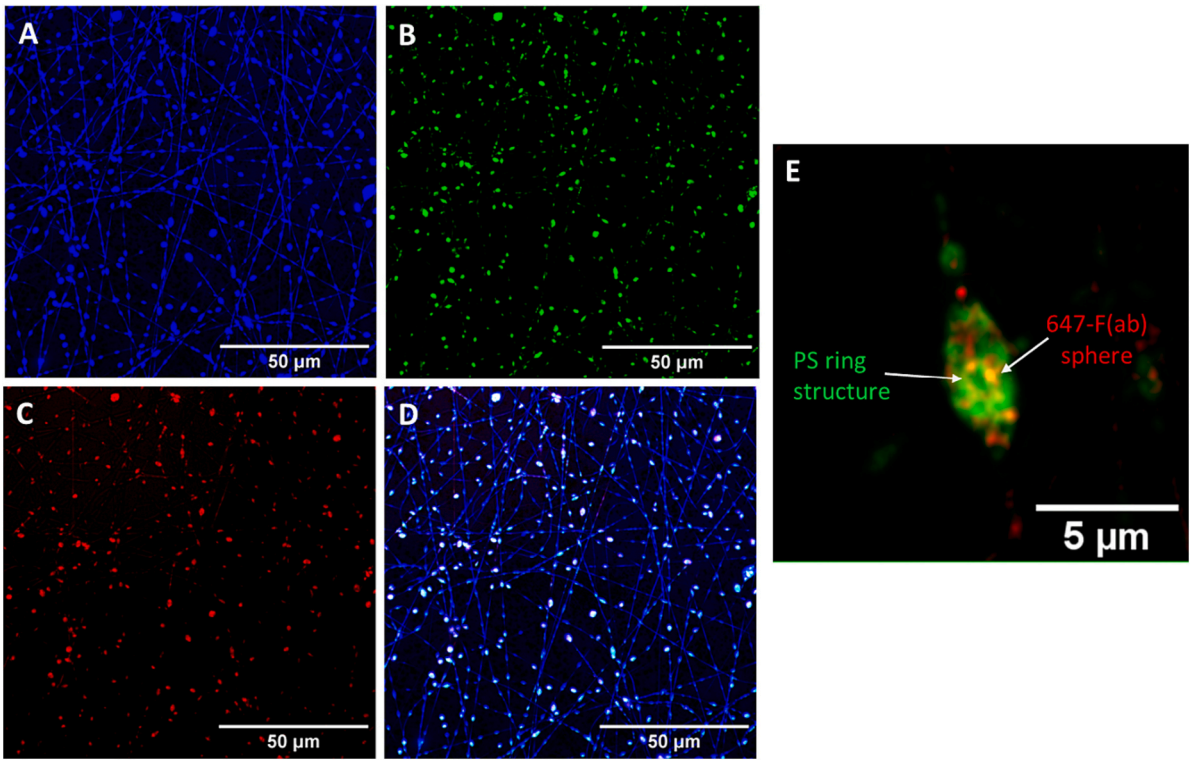

Fig. 3. Representative confocal images of fluorescent-labelled 647-F(ab)-PS membranes. Thin layers of electrospun material were collected on glass coverslips and imaged by super-resolution confocal imaging. Images of fibres captured using multichromatic confocal microscopy (A) PS hydrophobic block labelled with rhodamine B (green), (B) 647-F(ab) (red), (C) 7-hydroxy-4-(trifluoromethyl)coumarin dye used as a contrast agent to show overall fibre structure (blue), (D) overlay. Scale bar = 50 μm (E) High magnification image showing optical cross section of an individual bead, captured using z-stack function in dual chromatic confocal microscopy. Scale bar = 5 μm. (For interpretation of the references to colour in this figure legend, the reader is referred to the web version of this article.)

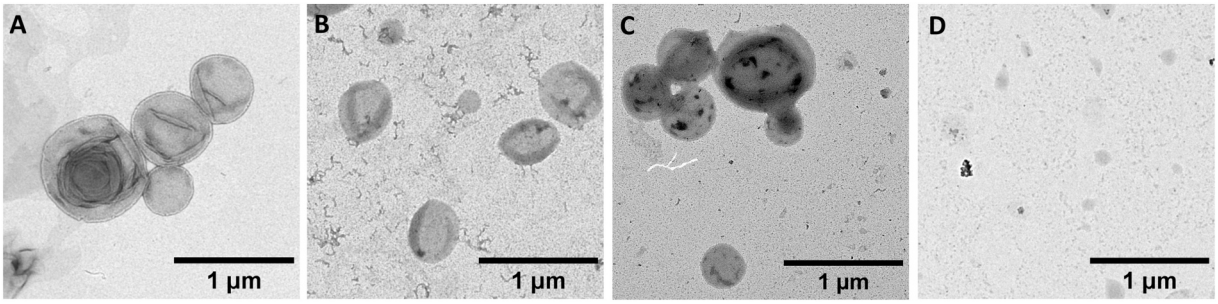

Fig. 4. Representative transmission electron micrographs of surface-adsorbed BSA-PS. (A) Crude PS-BSA following synthesis, (B) SEC-purified BSA-PS, (C) BSA-PS following electrospinning encapsulation and release by dissolving in deionised water, (D) PEO-only membranes were dissolved and used as a negative control. Scale bar = 1 μm.

Table 2
Hydrodynamic diameters of BSA-PS dispersions obtained using dynamic light scattering. Measurements were performed on crude BSA-PS following synthesis, after SEC-purification, and following electrospinning encapsulation and release by dissolution in PBS. Dissolved PEO-only membranes were included as a control. Values are presented as mean ± SD for 6 repeated measurements on a representative batch of BSA-PS.

	Crude	SEC-purified	Electrospun	PEO only
D_h (DLS)	390 ± 42 nm	387 ± 42 nm	340 ± 130 nm	42 ± 9 nm

3.7. Membrane delivery of polymersomes to reconstituted human oral epithelium

RHOE were used as a model oral epithelial barrier to investigate membrane delivery of PS to epithelial surfaces. The RHOE were 100–150 μm thick, which is comparable to the sublingual epithelium [28] with average TEER values of 1180 ± 350 Ω cm^2, indicating robust epithelial permeability barrier properties [29]. Electrospun membranes (10 mg) containing 647-F(ab)-PS or BSA-PS were applied to the apical surface of the RHOE along with PBS (0.5 mL) to simulate saliva within the oral cavity that dissolve the fibres. After 6 h topical application the rhodamine B-labelled PS component of 647-F(ab)-PS and BSA-PS was detectable several cell layers deep into the epithelium (within the upper 25–50 μm epithelial layers). For 647-F(ab)-PS, the F(ab) was detectable within the upper 1–2 cell layers and colocalised with the PS, suggesting successful delivery of the PS-encapsulated biologic into the epithelium (Fig. 6).

Table 3
Encapsulation efficiency (EE) calculations for B-F(ab)-PS in the crude PISA reaction product and in the final electrospun membrane. Enzyme-linked immunosorbent assay (ELISA) was used to quantify functional F(ab) concentrations through binding to surface immobilised mouse immunoglobulin. Encapsulated F(ab) was released by disrupting the PS vesicle morphology in ethanol. As controls BSA-PS solutions and membranes were analysed by ELISA, which resulted in negligible colour change. Data are presented as mean ± SD ($N = 3$).

	Crude	Electrospun
Theoretical F(ab) loading (ng/mg polymer)	474	220 ± 21
ELISA-measured Total F(ab) (ng/mg polymer)	366 ± 49	92 ± 30
ELISA-measured unencapsulated F(ab) (ng/mg polymer)	193 ± 34	28 ± 13
Calculated encapsulated F(ab) (ng/mg polymer)	173 ± 15	64 ± 17
Calculated % EE (Total)	36.5 ± 3.1	28.5 ± 5.1
Calculated % Activity loss (PISA)	23 ± 10	–
Calculated % EE (Electrospinning)	–	78 ± 13

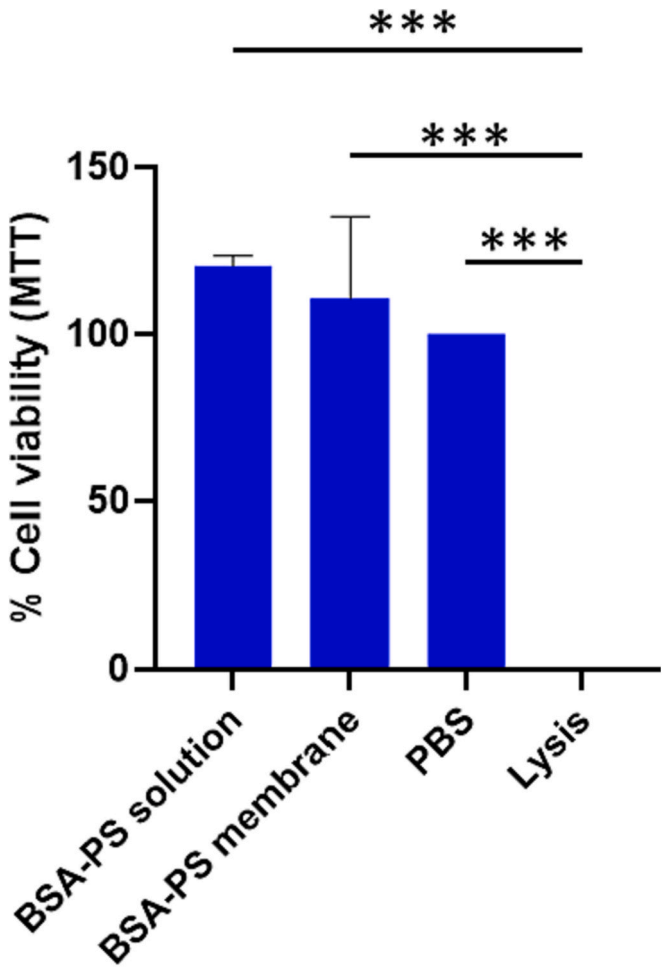

Fig. 5. Cytotoxicity testing of BSA-PS solutions and membranes measured using a tetrazolium dye (MTT) metabolic assay as an indirect measure of viability with reconstituted human oral epithelia (RHOE). Treatment with sodium dodecyl sulphate to cause total cell lysis was used as a control. Data are presented as mean ± SD; n = 3 and tested for significance using one-way ANOVA ($p < 0.0001$). ***, $p < 0.001$.

4. Discussion

Polymersomes (PS) are artificial hollow spheres formed by amphiphilic copolymers, most commonly in an aqueous solution [30]. Therefore, water was selected as a processing solvent to preserve their vesicular morphology. Aqueous PS at 2 % w/v could not be electrospun without added polymer. This is expected due to the lack of molecular entanglement between polymer vesicles, resulting in insufficient viscosity for fibre formation [31]. Electrospraying was also not observed due to the high surface tension of the aqueous solution. 600 kDa PEO was selected as a fibre-forming excipient because of its excellent electrospinning properties in water [32]. Furthermore, PEO is considered a biologically inert pharmaceutical-grade excipient with mucoadhesive properties [33], which make it promising for use in a topical mucosal drug delivery system, for example in the oral cavity [5]. Electrospinning of 2 % w/v empty-PS from an aqueous solution was achieved with the inclusion of 3 % w/v 600 kDa PEO but not with 5 or 10 % w/v PEO. Interestingly, by electrospinning PEO in the absence of PS, it was found that 3 % w/v PEO produces bead-on-string fibres, whereas 5, and 10 % w/v produce monolithic bead-free fibres, suggesting that a bead-on-string morphology may be an important feature to enable the electrospinning of PS. The electrospinning process was investigated further for the encapsulation of protein-loaded fluorescent PS, with the aim of developing a topical formulation for the delivery of biopharmaceutical-

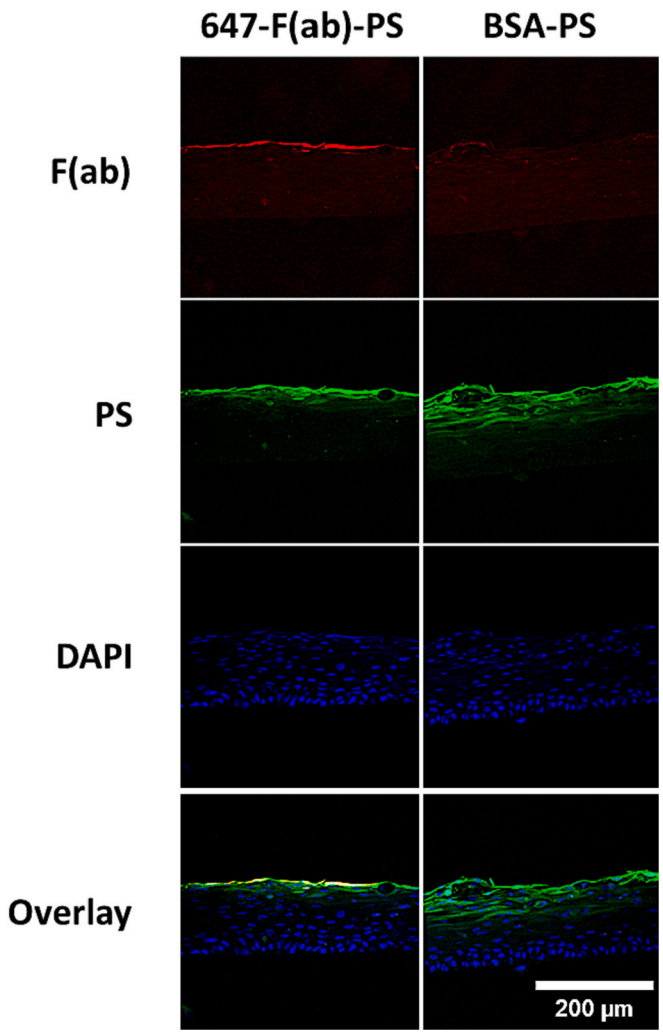

Fig. 6. Membrane delivery of 647-F(ab)-PS and BSA-PS to reconstituted human oral epithelia (RHOE) visualised using confocal microscopy. Membranes were applied to RHOE for 6 h before washing and formalin fixation to immobilise the polymer and protein. Cryosections were incubated with 4′,6-diamidino-2-phenylindole (DAPI) as a nuclear counterstain. AlexaFluor 647-labelled F(ab) (red), Rhodamine B-labelled polymer (green), DAPI nuclear counterstain (blue). Images shown are representative images of one experiment performed in triplicate. (For interpretation of the references to colour in this figure legend, the reader is referred to the web version of this article.)

loaded PS.

Changes in DSC and FTIR spectrum of the material were consistent with the incorporation of BSA-PS. The presence of BSA-PS reduced the tensile strength of the membranes. However, both PEO-only and BSA-PS membranes were ductile and easy to handle. With the inclusion of BSA-PS, the spindle-shaped beads of the membrane appeared bumpy when imaged using SEM, suggesting some heterogeneity within the beads. The fibres connecting the beads appeared smooth, suggesting that the PS may accumulate preferentially within the beads. Super-resolution confocal microscopy confirmed this hypothesis, showing rings of fluorescent polymer and spheres of 647-F(ab), verifying that the PS vesicle morphology was intact within the electrospun fibre and that multiple PS are encapsulated within each bead.

Bead-on-string electrospinning occurs as an intermediate between electrospinning and electrospraying and its occurrence is strongly influenced by the viscosity, charge density, and surface tension of the polymer solution [34]. When surface tension is high relative to viscosity, beads are favoured to minimise surface energy. During bead-on-string electrospinning, charged droplets containing coiled and weakly-overlapping macromolecules of dissolved polymer are ejected following Plateau-Rayleigh breakup of the cone jet. Fong et al theorised that the high extensional flow at the point of Plateau-Rayleigh break-up causes the alignment and overlap the of polymer macromolecules, producing fibrils of shear-thickened polymer solution that connect the beads and persist as the jet solidifies [34]. This is supported by Dunderdale et al who showed that aqueous PEO solutions subjected to high

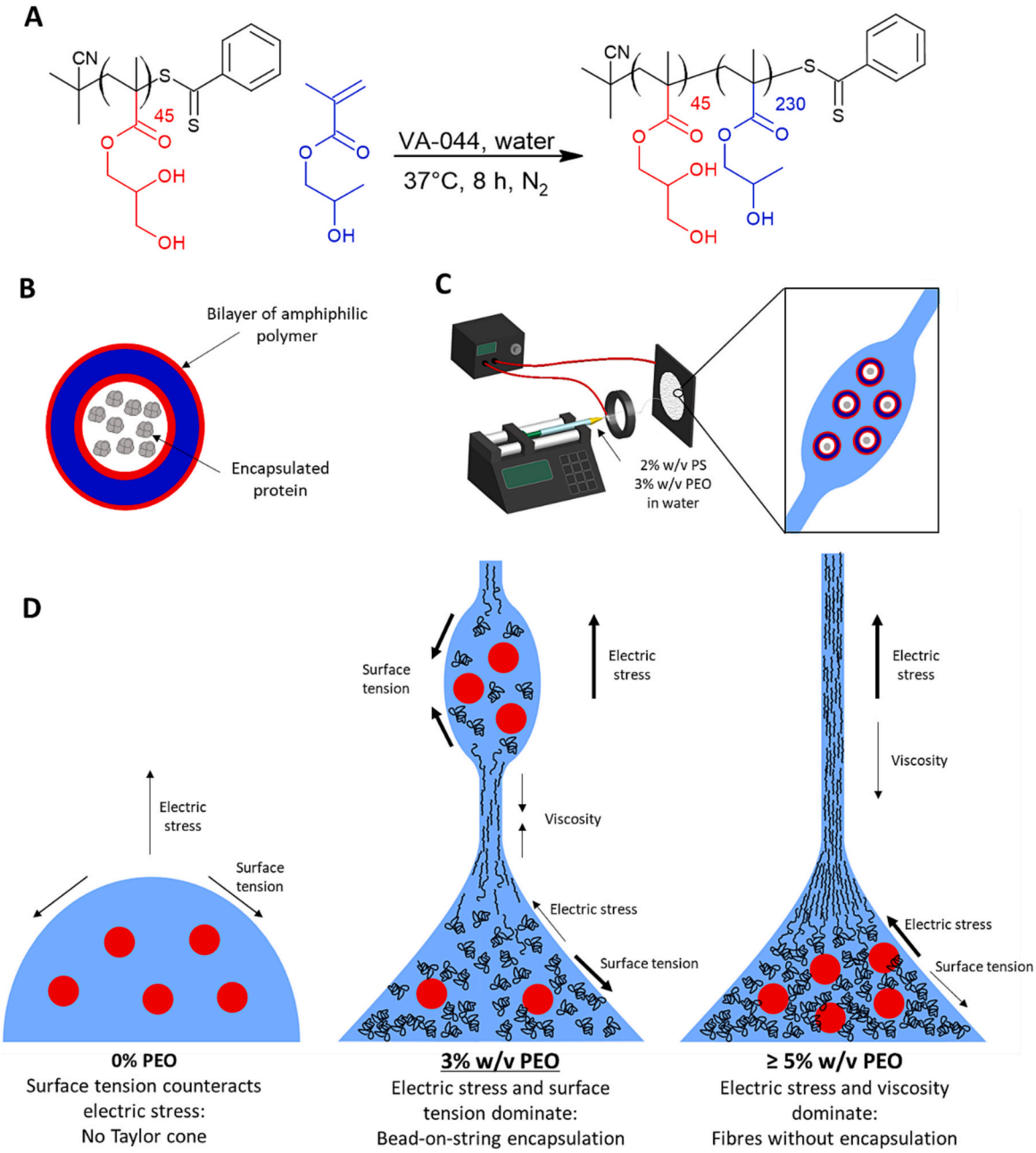

Fig. 7. Schematic diagram illustrating the synthesis, purification, and electrospinning encapsulation of protein-loaded PS. (A) Synthesis of PGMA-PHPMA PS via RAFT aqueous emulsion polymerization at 37 °C. (B) Proteins are encapsulated within the PS lumen in situ during polymer synthesis (C) Unencapsulated protein is removed using size exclusion chromatography yielding a 2–3 % w/v polymer dispersion before adding 3 % w/v PEO 600 kDa and electrospinning into bead-on-string fibres. (D) Illustration of the hypothesized mechanism for the superior electrohydrodynamic encapsulation of PS within bead-on-string fibres, with arrows showing the forces involved at the point of ejection from the Taylor cone.

shear can undergo a flow-induced crystallisation, whereby PEO macromolecules undergo transition from a hydrated globular structure to an aligned dehydrated state [35]. Our hypothesis is that PS could not be encapsulated using conventional electrospinning into smooth PEO fibres due to the PEO macromolecules aligning and hydrogen bonding together at high shear, creating a siphon effect which excludes PS from the electrospinning jet (Fig. 7D). In contrast, low shear stress (and consequently lower degree of molecular entanglement within beads during bead-on-string electrospinning) promotes encapsulation, causing PS to accumulate within beads and to be excluded from the interconnecting fibrils. Beaded fibres have often been considered to be a defective by-product of the electrospinning process with few practical applications [36,37]. To our knowledge, this is the first report of bead-on-string electrospinning being used to encapsulate difficult-to-electrospin materials.

TEM imaging and DLS showed intact vesicular morphology of BSA-PS following release from the electrospun fibre. B-F(ab) was encapsulated as a model functional protein to investigate the suitability of the formulation for biopharmaceutical delivery and to quantify electrospinning encapsulation efficiency. F(ab) was encapsulated within PS with an EE of 36.5 ± 3.1 % which is somewhat higher than expected based on previous studies of encapsulation using PISA [21], suggesting that the F(ab) may hydrogen bond to the polymers during synthesis and become enriched within the PS lumen and/or membrane. 78 ± 13 % of the F(ab) remained encapsulated within PS and retained antigen-binding functionality following electrospinning and release from the membrane fibres. These results confirm that PS vesicle morphology remains intact, and that the majority of the vesicle contents are retained during electrospinning and PS release from the fibres. Electrospinning was also non-denaturing, suggesting suitability for biopharmaceutical delivery. Several previous studies report electrospinning for the encapsulation of PS or other synthetic vesicles where these remain permanently immobilised within the fibres and are not released [19,38]. Two studies report the elution of liposomes from electrospun fibres [39,40], although the encapsulation of vesicle contents following release from the fibres has not been measured previously. To our knowledge, this work is the first report of an electrospun material for the release of intact PS. Furthermore, the high vesicle content of at least 30 % *w*/w PS by polymer mass (according to NMR analysis), suggests that the membranes reported here may be particularly applicable for topical drug delivery, for which high loading of active ingredients is often required.

BSA-PS applied either as a solution or in a PEO membrane were found to be non-irritant to the oral epithelium in a tissue engineered model. The ability of the membranes to deliver PS to oral epithelia was assessed using fluorescence imaging. After applying membranes for 6 h, PS was detectable within the apical epithelium indicating their suitability as drug delivery vehicles. Similar data was observed by Hearnden et al who assessed uptake of PEO-functionalised polymersomes in tissue engineered models of the oral mucosa [41]. PEO is often used as a 'stealth' coating for PS and other nanomedicines. The PGMA used in this study was intended to have a similar role as a biologically inert surface polymer that promotes passive diffusion through the tissue. Indeed, the extent of epithelial permeation in this study was comparable to that previously observed for PEO-functionalised PS [41].

Following delivery of 647-F(ab)-PS into RHOE, the fluorescent-conjugated F(ab) colocalised with the PS, suggesting successful uptake of the 647-F(ab) alongside the PS by epithelial cells. Although this study presents a formulation that successfully delivers biologic-loaded PS to epithelial tissue, further research is required to optimise PS chemistry for improved tissue permeation and to allow targeted release of a biologic that provides a therapeutic function within epithelial cells, such as plasmid-based therapy or intracellular-cytokine-neutralising antibody [25,42]. Uptake of nanomedicines is often mediated by endocytosis, which risks lysosomal degradation of encapsulated biopharmaceuticals, although transcytosis or passive diffusion may also occur [43]. Mable et al achieved intracellular DNA delivery in breast cancer cells using similar PGMA-PHPMA-based PS by introducing pH-responsive groups within the hydrophobic polymer block [44]. Following endocytosis and compartmentalisation at low pH, the PS disassemble, causing release of the encapsulated DNA and rupture of the endosomal membrane. As part of a portfolio of studies, Armes and co-workers have introduced various features into PGMA-PHPMA PS including temperature-/pH-responsiveness [21,45], mucoadhesion [46], and cellular targeting [44]. Other groups have also produced PS with a wide variety of stimuli-responsive release and cell targeting mechanisms [47,48]. This demonstrates the modularity of PS technology and provides a toolkit to further develop the formulation for targeted biologic delivery.

5. Conclusion

Here, we report here the first electrospun formulation for the delivery of biologic-loaded PS. The F(ab) model biologic remained functional and encapsulated within the polymer vesicles following release from the fibrous material. Uniquely, the fabrication process of bead-on-string electrospinning generated an accumulation of PS within the beads, providing a new strategy for the efficient electrospinning encapsulation of complex nanostructured carriers. The resulting membranes were non-irritant and delivered detectable levels of PS within oral epithelia when applied topically. These data demonstrate a promising new technology for the delivery of therapeutic PS to mucosal surfaces.

Statement of significance

Electrospinning technology has been used to fabricate highly mucoadhesive membranes for the topical delivery of small molecules to the mucosal epithelium, but further development is required for delivery of vesicular vectors such as polymersomes that allow administration of advanced therapeutics. Herein, we load polymersome vesicles with antibody f(ab) fragments as a model biotherapeutic and incorporate these into electrospun fibres to create bead-on-string fibre-containing membranes. Results show, for the first time, polymersome release from bead-on-string fibres with intact vesicle morphology and release of biotherapeutic with maintained functionality into tissue-engineered mucosal epithelium. This novel membrane formulation could form the basis for new therapeutic delivery strategies to treat a variety of mucosal conditions.

CRediT authorship contribution statement

Jake G. Edmans: Conceptualization, Data curation, Formal analysis, Investigation, Methodology, Validation, Visualization, Writing – original draft. **Samuel Harrison:** Investigation. **Paul V. Hatton:** Conceptualization, Supervision, Writing – review & editing, Funding acquisition. **Craig Murdoch:** Conceptualization, Supervision, Writing – review & editing. **Sebastian G. Spain:** Conceptualization, Supervision. **Helen E. Colley:** Conceptualization, Funding acquisition, Methodology, Project administration, Supervision, Writing – review & editing.

Declaration of competing interest

JGE, SH, CM, SS and HEC declare that they have no other known competing financial interests or personal relationships that could influence the work reported within this paper. PVH is on the AFYX Therapeutics APS scientific advisory board, where AFYX have translated mucoadhesive electrospun patch technology for clinical use and have intellectual property (international patent applications WO 2017/085262 A, WO 2021/072113 A1).

Data availability

Data will be made available on request.

Acknowledgements

The authors would like to thank Dr. Izzy Jayasinghe and Dr. Tom Sheard for helpful discussions on super-resolution microscopy, Christopher Hill of the Cryo-Electron Microscopy Facility and Cerys Evans for assistance in acquiring scanning electron microscopy images. Fluorescence imaging work was performed at the Wolfson Light Microscope Facility, which is supported by the Biotechnology and Biological Sciences Research Council (grant number BB/M012522/1). Funding: This work was funded by the Engineering and Physical Sciences Research Council (grant number EP/L016281/1) as a CASE PhD studentship (for JGE) with the Centre for Doctoral Training in Polymers, Soft Matter & Colloids, where AFYX Therapeutics (Copenhagen, Denmark) was the industrial sponsor. Additional funding was provided by an Engineering and Physical Sciences Research Council Impact Acceleration Award to HEC.

Appendix A. Supplementary data

Supplementary data to this article can be found online at https://doi.org/10.1016/j.bioadv.2023.213734.

References

[1] M.A. Gonzalez-Moles, S. Warnakulasuriya, I. Gonzalez-Ruiz, L. Gonzalez-Ruiz, A. Ayen, D. Lenouvel, I. Ruiz-Avila, P. Ramos-Garcia, Worldwide prevalence of oral lichen planus: a systematic review and meta-analysis, Oral Dis. 27 (2021) 813–828.
[2] A. El-Howati, M.H. Thornhill, H.E. Colley, C. Murdoch, Immune mechanisms in oral lichen planus, Oral Dis. 29 (2023) 1400–1415.
[3] A. Argiris, M.V. Karamouzis, D. Raben, R.L. Ferris, Head and neck cancer, Lancet 371 (2008) 1695–1709.
[4] V. Hearnden, V. Sankar, K. Hull, D.V. Juras, M. Greenberg, A.R. Kerr, P. B. Lockhart, L.L. Patton, S. Porter, M.H. Thornhill, New developments and opportunities in oral mucosal drug delivery for local and systemic disease, Adv. Drug Deliv. Rev. 64 (2012) 16–28.
[5] J.G. Edmans, K.H. Clitherow, C. Murdoch, P.V. Hatton, S.G. Spain, H.E. Colley, Mucoadhesive electrospun fibre-based technologies for oral medicine, Pharmaceutics 12 (2020).
[6] H.S. Sofi, A. Abdal-Hay, S. Ivanovski, Y.S. Zhang, F.A. Sheikh, Electrospun nanofibers for the delivery of active drugs through nasal, oral and vaginal mucosa: current status and future perspectives, Mater. Sci. Eng. C Mater. Biol. Appl. 111 (2020), 110756.
[7] U. Angkawinitwong, S. Awwad, P.T. Khaw, S. Brocchini, G.R. Williams, Electrospun formulations of bevacizumab for sustained release in the eye, Acta Biomater. 64 (2017) 126–136.
[8] H.E. Colley, Z. Said, M.E. Santocildes-Romero, S.R. Baker, K. D'Apice, J. Hansen, L. S. Madsen, M.H. Thornhill, P.V. Hatton, C. Murdoch, Pre-clinical evaluation of novel mucoadhesive bilayer patches for local delivery of clobetasol-17-propionate to the oral mucosa, Biomaterials 178 (2018) 134–146.
[9] M.T. Brennan, L.S. Madsen, D.P. Saunders, J.J. Napenas, C. McCreary, R. Ni Riordain, A.M.L. Pedersen, S. Fedele, R.J. Cook, R. Abdelsayed, M.T. Llopiz, V. Sankar, K. Ryan, D.A. Culton, Y. Akhlef, F. Castillo, I. Fernandez, S. Jurge, A. R. Kerr, C. McDuffie, T. McGaw, A. Mighell, T.P. Sollecito, T. Schlieve, M. Carrozzo, A. Papas, T. Bengtsson, I. Al-Hashimi, L. Burke, N.W. Burkhart, S. Culshaw, B. Desai, J. Hansen, P. Jensen, T. Menne, P.B. Patel, M. Thornhill, N. Treister, T. Ruzicka, Efficacy and safety of a novel mucoadhesive clobetasol patch for treatment of erosive oral lichen planus: a phase 2 randomized clinical trial, J. Oral Pathol. Med. 51 (2022) 86–97.
[10] S.S. Ibrahim, N.I. Ragy, N.A. Nagy, H. El-Kammar, A.M. Elbakry, O.M. Ezzatt, Evaluation of muco-adhesive tacrolimus patch on caspase-3 induced apoptosis in oral lichen planus: a randomized clinical trial, BMC Oral Health 23 (2023) 99.
[11] T. Caon, L. Jin, C.M. Simoes, R.S. Norton, J.A. Nicolazzo, Enhancing the buccal mucosal delivery of peptide and protein therapeutics, Pharm. Res. 32 (2015) 1–21.
[12] H.E. Colley, V. Hearnden, M. Avila-Olias, D. Cecchin, I. Canton, J. Madsen, S. MacNeil, N. Warren, K. Hu, J.A. McKeating, S.P. Armes, C. Murdoch, M. H. Thornhill, G. Battaglia, Polymersome-mediated delivery of combination anticancer therapy to head and neck cancer cells: 2D and 3D in vitro evaluation, Mol. Pharm. 11 (2014) 1176–1188.
[13] E.C. Lavelle, R.W. Ward, Mucosal vaccines - fortifying the frontiers, Nat. Rev. Immunol. 22 (2022) 236–250.
[14] I. Canton, M. Massignani, N. Patikarnmonthon, L. Chierico, J. Robertson, S. A. Renshaw, N.J. Warren, J.P. Madsen, S.P. Armes, A.L. Lewis, G. Battaglia, Fully synthetic polymer vesicles for intracellular delivery of antibodies in live cells, FASEB J. 27 (2013) 98–108.
[15] D.A. Christian, S. Cai, D.M. Bowen, Y. Kim, J.D. Pajerowski, D.E. Discher, Polymersome carriers: from self-assembly to siRNA and protein therapeutics, Eur. J. Pharm. Biopharm. 71 (2009) 463–474.
[16] S. Kansiz, Y.M. Elcin, Advanced liposome and polymersome-based drug delivery systems: considerations for physicochemical properties, targeting strategies and stimuli-sensitive approaches, Adv. Colloid Interf. Sci. 317 (2023), 102930.
[17] J. Zhang, L. Wu, F. Meng, Z. Wang, C. Deng, H. Liu, Z. Zhong, pH and reduction dual-bioresponsive polymersomes for efficient intracellular protein delivery, Langmuir 28 (2012) 2056–2065.
[18] W. Ji, F. Yang, J.J. van den Beucken, Z. Bian, M. Fan, Z. Chen, J.A. Jansen, Fibrous scaffolds loaded with protein prepared by blend or coaxial electrospinning, Acta Biomater. 6 (2010) 4199–4207.
[19] M.C. Sanchez-Cervino, C.P. Fuioaga, L.I. Atanase, G.A. Abraham, G. Rivero, Electrohydrodynamic techniques for the manufacture and/or immobilization of vesicles, Polymers (Basel) 15 (2023).
[20] J. Masek, D. Lubasova, R. Lukac, P. Turanek-Knotigova, P. Kulich, J. Plockova, E. Maskova, L. Prochazka, S. Koudelka, N. Sasithorn, J. Gombos, E. Bartheldyova, F. Hubatka, M. Raska, A.D. Miller, J. Turanek, Multi-layered nanofibrous mucoadhesive films for buccal and sublingual administration of drug-delivery and vaccination nanoparticles - important step towards effective mucosal vaccines, J. Control. Release 249 (2017) 183–195.
[21] C.J. Mable, R.R. Gibson, S. Prevost, B.E. McKenzie, O.O. Mykhaylyk, S.P. Armes, Loading of silica nanoparticles in block copolymer vesicles during polymerization-induced self-assembly: encapsulation efficiency and thermally triggered release, J. Am. Chem. Soc. 137 (2015) 16098–16108.
[22] M.E. Santocildes-Romero, L. Hadley, K.H. Clitherow, J. Hansen, C. Murdoch, H. E. Colley, M.H. Thornhill, P.V. Hatton, Fabrication of electrospun mucoadhesive membranes for therapeutic applications in oral medicine, ACS Appl. Mater. Interfaces 9 (2017) 11557–11567.
[23] J.G. Edmans, C. Murdoch, M.E. Santocildes-Romero, P.V. Hatton, H.E. Colley, S. G. Spain, Incorporation of lysozyme into a mucoadhesive electrospun patch for rapid protein delivery to the oral mucosa, Mater. Sci. Eng. C Mater. Biol. Appl. 112 (2020), 110917.
[24] C.A. Schneider, W.S. Rasband, K.W. Eliceiri, NIH Image to ImageJ: 25 years of image analysis, Nat. Methods 9 (2012) 671–675.
[25] J.G. Edmans, B. Ollington, H.E. Colley, M.E. Santocildes-Romero, L. Siim Madsen, P.V. Hatton, S.G. Spain, C. Murdoch, Electrospun patch delivery of anti-TNFalpha F (ab) for the treatment of inflammatory oral mucosal disease, J. Control. Release 350 (2022) 146–157.
[26] L.R. Jennings, H.E. Colley, J. Ong, F. Panagakos, J.G. Masters, H.M. Trivedi, C. Murdoch, S. Whawell, Development and characterization of in vitro human oral mucosal equivalents derived from immortalized oral keratinocytes, Tissue Eng. Part C Methods 22 (2016) 1108–1117.
[27] I.J. Pucic, T., FTIR assessment of poly(ethylene oxide) irradiated in solid state, melt and aqeuous solution, Radiat. Phys. Chem. 81 (2012) 1426–1429.
[28] S. Prestin, S.I. Rothschild, C.S. Betz, M. Kraft, Measurement of epithelial thickness within the oral cavity using optical coherence tomography, Head Neck 34 (2012) 1777–1781.
[29] L. Bierbaumer, U.Y. Schwarze, R. Gruber, W. Neuhaus, Cell culture models of oral mucosal barriers: a review with a focus on applications, culture conditions and barrier properties, Tissue Barriers 6 (2018), 1479568.
[30] S. Iqbal, M. Blenner, A. Alexander-Bryant, J. Larsen, Polymersomes for therapeutic delivery of protein and nucleic acid macromolecules: from design to therapeutic applications, Biomacromolecules 21 (2020) 1327–1350.
[31] N. Bhardwaj, S.C. Kundu, Electrospinning: a fascinating fiber fabrication technique, Biotechnol. Adv. 28 (2010) 325–347.
[32] B. Duan, C. Dong, X. Yuan, K. Yao, Electrospinning of chitosan solutions in acetic acid with poly(ethylene oxide), J. Biomater. Sci. Polym. Ed. 15 (2004) 797–811.
[33] D. Tiwari, D. Goldman, R. Sause, P.L. Madan, Evaluation of polyoxyethylene homopolymers for buccal bioadhesive drug delivery device formulations, AAPS PharmSci. 1 (1999) E13.
[34] H.C. Fong, I., D.H. Reneker, Beaded nanofibres formed during electrospinning, Polymer 40 (1999) 4585–4592.
[35] G.J. Dunderdale, S.J. Davidson, A.J. Ryan, O.O. Mykhaylyk, Flow-induced crystallisation of polymers from aqueous solution, Nat. Commun. 11 (2020) 3372.
[36] W. Chen, P. Zhao, Y. Yang, D.G. Yu, Electrospun beads-on-the-string nanoproducts: preparation and drug delivery application, Curr. Drug Deliv. 20 (2023) 1224–1240.
[37] H.C. Zhao, H., Elecrtospun Bead-on-String Fibers: Useless or Something of Value, IntechOpen, United Kingdom, 2018.
[38] B.P. Nair, D. Vaikkath, D.S. Mohan, P.D. Nair, Fabrication of a microvesicles-incorporated fibrous membrane for controlled delivery applications in tissue engineering, Biofabrication 6 (2014), 045008.
[39] R.H. de Freitas Zompero, A. Lopez-Rubio, S.C. de Pinho, J.M. Lagaron, L.G. de la Torre, Hybrid encapsulation structures based on beta-carotene-loaded nanoliposomes within electrospun fibers, Colloids Surf. B: Biointerfaces 134 (2015) 475–482.
[40] R.P.R. Trindade, N., N. El Harane, P. Menache, G.R. Williams, Extracellular vesicles can be processed by electrospinning without loss of structure or function, Mater. Lett. 282 (2021), 128671.
[41] V. Hearnden, H. Lomas, S. Macneil, M. Thornhill, C. Murdoch, A. Lewis, J. Madsen, A. Blanazs, S. Armes, G. Battaglia, Diffusion studies of nanometer polymersomes across tissue engineered human oral mucosa, Pharm. Res. 26 (2009) 1718–1728.
[42] V. Sankar, V. Hearnden, K. Hull, D.V. Juras, M.S. Greenberg, A.R. Kerr, P. B. Lockhart, L.L. Patton, S. Porter, M. Thornhill, Local drug delivery for oral mucosal diseases: challenges and opportunities, Oral Dis. 17 (Suppl. 1) (2011) 73–84.
[43] I. Canton, G. Battaglia, Endocytosis at the nanoscale, Chem. Soc. Rev. 41 (2012) 2718–2739.

[44] C.J.C. Mable, I., O.O. Mykhaylyk, B. Ustbas Gul, P. Chambon, E. Themistou, S. P. Armes, Targeting triple-negative breast cancer cells using Dengue virus-mimicking pH-responsive framboidal triblock copolymer vesicles, Chem. Sci. 10 (2019) 4811–4821.
[45] C.J. Mable, L.A. Fielding, M.J. Derry, O.O. Mykhaylyk, P. Chambon, S.P. Armes, Synthesis and pH-responsive dissociation of framboidal ABC triblock copolymer vesicles in aqueous solution, Chem. Sci. 9 (2018) 1454–1463.
[46] E.E. Brotherton, M.J. Smallridge, S.P. Armes, Aldehyde-functional diblock copolymer nano-objects via RAFT aqueous dispersion polymerization, Biomacromolecules 22 (2021) 5382–5389.
[47] X. Hu, Y. Zhang, Z. Xie, X. Jing, A. Bellotti, Z. Gu, Stimuli-responsive polymersomes for biomedical applications, Biomacromolecules 18 (2017) 649–673.
[48] H. Moulahoum, F. Ghorbanizamani, F. Zihnioglu, S. Timur, Surface biomodification of liposomes and polymersomes for efficient targeted drug delivery, Bioconjug. Chem. 32 (2021) 1491–1502.